Investigation of photocatalytic performance of CuS/Bi_2WO_6 and degradation pathway of RhB in water

Houren Zhou, Jiaxiu Guo, Ningjie Fang, Juan Liang, Ting Shen and Shandong Yuan

ABSTRACT

A series of CuS/Bi_2WO_6 composites were synthesized by solvothermal synthesis, which showed enhanced photocatalytic activity. The as-prepared samples were characterized by X-ray diffraction, scanning electron microscopy, high-resolution transmission electron microscopy, photoluminescence ultraviolet–visible absorption spectroscopy, transient photocurrent and EIS. The results showed that as-prepared CuS/Bi_2WO_6 has flower-like nano microspheres self-assembled by nanoplates and CuS nanorods are uniformly dispersed on its surface. The CuS/Bi_2WO_6 forms heterojunctions between CuS and Bi_2WO_6 and shows a wide light response range and a strong light response intensity. The CuS/Bi_2WO_6 exhibits a better Rhodamine B (RhB) degradation effect than pure Bi_2WO_6 and CuS, and it can degrade 90% RhB in 50 min and achieve complete degradation in 70 min under Xe lamp irradiation. The CuS/Bi_2WO_6 has photocatalytic activity in a low pH environment and good stability. The formation of a heterojunction between CuS and Bi_2WO_6 can effectively separate photo-generated electrons and holes, greatly improving the photocatalytic activity. In the CuS/Bi_2WO_6-RhB reaction system, O_2^- is the main active species, and it can rapidly remove the ethyl group from the amino group linked to benzene rings to achieve the N-de-ethylation reaction in the process of RhB degradation. The N-de-ethylated products are simultaneously degraded to small organic molecules and even mineralized into CO_2 and H_2O.

Key words | CuS/Bi_2WO_6, heterojunction, photocatalyst, RhB degradation

Houren Zhou
Ningjie Fang
Juan Liang
Ting Shen
College of Architecture and Environment,
Sichuan University,
Chengdu 610065, Sichuan,
China

Jiaxiu Guo (corresponding author)
Shandong Yuan
National Engineering Technology Research Center for Flue Gas Desulfurization, Chengdu 610065, Sichuan,
China
and
Institute of New Energy and Low Carbon Technology,
Sichuan University,
Chengdu 610065, Sichuan,
China
E-mail: *guojiaxiu@scu.edu.cn*

INTRODUCTION

Pharmaceutical, printing and dyeing, papermaking and other industrial organic wastewater discharge large quantities and contain a large number of refractory pollutants. These pollutants can have adverse effects on human health, damage the water ecological environment and seriously affect the utilization of water resources (Musikavong *et al.* 2005; Lefebvre & Moletta 2006). Photocatalytic technology, using semiconductor photocatalytic materials, can convert solar energy into chemical energy or electric energy to effectively remove organic pollutants in water under mild reaction conditions. It is one of the most promising technologies to solve energy and environmental problems (Herrmann *et al.* 1993; Chong *et al.* 2010). In recent years, in order to improve the photocatalytic activity and stability of semiconductor catalytic materials, many researchers have worked to develop new photocatalytic materials, such as Bi_2WO_6 (Zhang *et al.* 2010), MoSe (Shi *et al.* 2013), Fe_2O_3 (Li *et al.* 2007), CdS (Li *et al.* 2009) and $ZnSn(OH)_6$ (Dong *et al.* 2019a). However, many studies have shown that it is often difficult to achieve perfect photocatalytic effect with a single photocatalyst. Therefore, some measures have been used by many researchers to modify photocatalysts to enhance photocatalytic performance. Ismail *et al.* (2013) have found that the photocatalytic activity

doi: 10.2166/aqua.2020.121

of TiO_2 is enhanced when precious metals are deposited on its surfaces. CdS nanometric particles, as a narrow band gap semiconducting material, were impregnated onto TiO_2 by Juliana *et al.* to optimize its photocatalytic properties (Tristão *et al.* 2006).

Recently, Bi_2WO_6 can photolyse water and degrade organic pollutants under visible light irradiation and has been a hot research topic in the field of photocatalysis (Tang *et al.* 2016; Zheng *et al.* 2017; Wan *et al.* 2018). However, Bi_2WO_6 is not stable and can be easily decomposed into tungstic acid under acidic conditions (Zheng *et al.* 2011). For CuS, the band gap is 1.76–2.48 eV, and it has a certain photocatalytic performance (Ding *et al.* 2008; Saranya *et al.* 2015). However, the response of CuS to light and the transfer efficiency of photo-generated carriers are not very high in the photocatalytic reaction (Chen *et al.* 2016). This makes it difficult to meet the requirements of practical application. Therefore, it is necessary to develop new photocatalysts. The study has shown that optical properties of a single semiconductor can be improved by combining P-type semiconductors with N-type semiconductors to form a heterojunction structure (Würthner *et al.* 2004). Many photocatalysts with a heterojunction structure, such as Bi_2WO_6@RGO (Dong *et al.* 2017), graphene@Bi_2WO_6 (Dong *et al.* 2019b), $AgNbO_3$@g-C_3N_4 (Chen *et al.* 2019a), g-C_3N_4@$Bi_4O_5I_2$ (Feng *et al.* 2020) and SnSe@g-C_3N_4 (Chen *et al.* 2019b), have been synthesized. Bi_2WO_6 is a wide band gap N-type semiconductor with a band gap of 2.69–2.75 (Kuchment & Kunyansky 1999), while CuS is a P-type semiconductor (Inoue *et al.* 2001). The combination of Bi_2WO_6 and CuS may form a P–N heterojunction. This structure can greatly improve the efficiency of photocatalytic carrier transmission, causing an increase of the photocatalytic rate (Oregan & Schwartz 1996). Therefore, the goal of this work is to synthesize a novel CuS/Bi_2WO_6 photocatalyst with the heterojunction structure using the hydrothermal method from sodium tungstate, bismuth nitrate, copper acetate and thiourea as precursors. It is more important to study its photocatalytic enhancement and photodegradation conditions, as well as the degradation pathway for RhB.

In this paper, a novel CuS/Bi_2WO_6 photocatalyst was synthesized by solvent hydrothermal synthesis. As comparative samples, Bi_2WO_6 and CuS were also prepared. The as-prepared samples were characterized by X-ray diffraction (XRD), scanning electron microscopy (SEM), high-resolution transmission electron microscopy (HRTEM), photoluminescence (PL) and ultraviolet–visible absorption spectroscopy (UV–Vis). The photocatalytic degradation conditions of Rhodamine B (RhB) were involved.

EXPERIMENTAL

Materials

Bismuth nitrate pentahydrate ($Bi(NO_3)_3{\cdot}5H_2O$; AR grade), sodium tungsten dihydrate ($Na_2WO_6{\cdot}2H_2O$; AR grade), copper acetate ($Cu(AC)_2$; AR grade), ethanol (AR grade), ethylene glycol (AR grade), sodium hydroxide (AR grade), nitric acid (HNO_3; AR grade) and thiourea (AR grade) were purchased from Chengdu Kelong Chemical Reagent Factory in Chengdu, China. All chemicals were used as received without further purification. The deionized water used throughout the experiments was prepared using an ULUPURVERY water system.

Instrumentation

SEM (Hitachi S-4700; Japan) and HRTEM (Tecnai G2 F20 Super Twin; USA) were used to examine the morphologies and structures of the samples. The optical properties were determined by UV–Vis diffuse reflectance spectroscopy (UV–vis DRS, Shimadzu UV-2600; Japan). XRD (X'Pert-Pro MPD; Holland Panalytical) was performed to analyze the crystal phase. The PL spectra of the samples were recorded by using a fluorescence spectrophotometer (Hitachi F-7100; Japan) with an excitation wavelength of 350 nm. The electron spin-resonance (ESR) spectroscopy was studied on a Bruker EMXplus X-band electron paramagnetic resonance spectrometer.

Synthesis of Bi_2WO_6

$Bi(NO_3)_3{\cdot}5H_2O$ and $Na_2WO_6{\cdot}2H_2O$ were the raw materials; the Bi_2WO_6 microspheres were prepared by a hydrothermal process. Firstly, 9.701 g $Bi(NO_3)_3{\cdot}5H_2O$ was dissolved in 40 mL deionized water under constant stirring

to form an aqueous solution, and 3.299 g $Na_2WO_6{\cdot}2H_2O$ was added into this aqueous solution. Secondly, after stirring for 30 min, the pH value of the mixture was adjusted to 1 using NaOH solution with 0.1 mol/L concentration. The resulting solution was then transferred to a 100 mL Teflon autoclave keeping it at 150 °C for 18 h. Finally, when the reactor was naturally cooled to room temperature, the precipitate was centrifuged, washed with ethanol and deionized water several times, and dried under vacuum at 110 °C for 3 h.

Synthesis of CuS

Typically, when 0.597 g $Cu(AC)_2$ was dissolved in 50 mL of ethylene glycol, a green color solution was formed. About 0.912 g thiourea was added into this solution with vigorous stirring. After stirring for 1 h, the solution was transferred to a 250 mL Teflon-lined autoclave. The autoclave was sealed and kept at 160 °C for 2 h. When the resulting solution was allowed to cool down to room temperature naturally, the solution was centrifuged. The obtained precipitate was washed with distilled water and ethanol. The resulting product was dried in a vacuum at 80 °C to obtain the final CuS product.

Synthesis of CuS/Bi_2WO_6

The CuS/Bi_2WO_6 sample was synthesized by a solvothermal reaction from Bi_2WO_6 powder and precursors of CuS from $Cu(AC)_2$ and thiourea. Firstly, 0.05 g $Cu(AC)_2$ and 0.076 g thiourea were, respectively, dissolved in 40 mL ethylene glycol under stirring. After stirring for 10 min, the glycol solution of thiourea was dripped slowly into the glycol solution of $Cu(AC)_2$ and continuously stirred. After that, 0.698 g of as-prepared Bi_2WO_6 was added into the solution mixture, and HNO_3 was used to adjust the pH value of the mixture to 4. After stirring for 30 min, the resulting mixtures were transferred into a 100 mL Teflon autoclave and kept at 150 °C for 12 h. After the reactor was naturally cooled to room temperature, the precipitate was centrifuged, washed several times using ethanol and deionized water and dried under vacuum at 80 °C. The CuS/Bi_2WO_6 sample was obtained. The molar mass ratio of CuS/Bi_2WO_6 is 1:4 and named as CBW1-4. According to the same preparation method, a series of samples were prepared by changing the mass ratio of CuS and Bi_2WO_6 to 2:1, 1:1, 1:2 and 1:6, and they were named CBW2-1, CBW1-1, CBW1-2 and CBW1-6, respectively.

Photocatalytic activity

Rhodamine B (RhB) was made into an aqueous solution to simulate actual dye wastewater. The adsorption and photocatalytic activity of as-prepared photocatalysts were evaluated by the degradation of RhB under the light irradiation by a 300 W Xe lamp (AuLight CEL-HXF300). In a typical experiment, 0.1 g photocatalysts were put into 150 mL RhB solution with a concentration of 20 mg/L in a quartz-glass reactor. To make sure that the RhB dye could reach the equilibrium of absorption–desorption on the surface of the photocatalyst, prior to irradiation, the suspension was stirred for 45 min at room temperature in the dark. Then, all procedures were carried out at room temperature under constant stirring. Three milliliters of the suspension was sampled in certain intervals and filtered, and the liquid was tested by UV–Vis spectroscopy (SHIMADZU UV-2600; Japan) according to its absorbance at 554 nm.

RESULTS

Characterization

Structure

XRD is often used to investigate the chemical structure of as-prepared samples. As shown in Figure 1, the synthesized samples have strong XRD diffraction peaks, indicating that the samples prepared under our experimental conditions have good crystallinity. In Figure 1(f) and 1(g), all the diffraction peaks can be readily assigned to the orthorhombic phase of Bi_2WO_6 (JCPDF card: 73-1126) and CuS (JCPDF card: 06-0464), respectively, and no peaks of impurity phase could be observed. These findings indicate that pure Bi_2WO_6 and CuS can be prepared under our experimental conditions. When CuS and Bi_2WO_6 are combined with different molar mass ratios, as shown in Figure 1(a)–1(e),

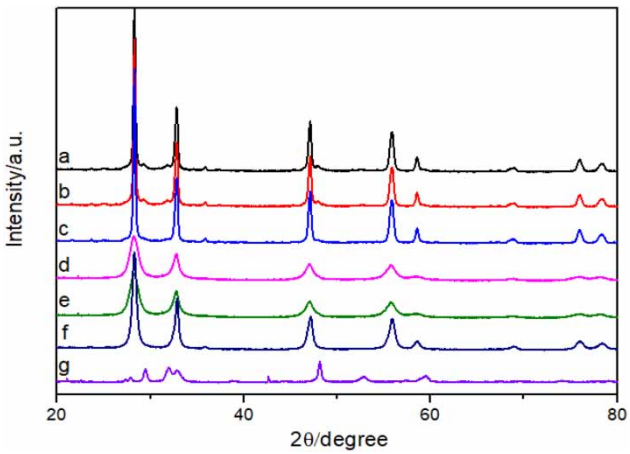

Figure 1 | XRD patterns of CBW1-6 (a), CBW1-4 (b), CBW1-2 (c), CBW1-1 (d), CBW2-1 (e), Bi_2WO_6 (f) and CuS (g).

the characteristic peak of CuS is not detected while characteristic diffraction peaks due to Bi_2WO_6 are clearly observed, and no significant shifts of the principal diffraction peaks are observed, indicating that CuS exists as a separate phase highly dispersed on the surface of Bi_2WO_6 rather than being incorporated into the Bi_2WO_6 lattice.

Morphology

SEM and HRTEM are used to determine the morphology and structure of the samples. In order to discover whether there is a new structure between CuS and Bi_2WO_6, the CBW1-4 sample is selected for HRTEM characterization. It can be clearly seen from Figure 2(a) that the prepared Bi_2WO_6 shows a flower-shaped sphere and its diameter is about 2–5 μm, indicating that the dispersion is uniform without agglomeration. This is in agreement with the literature (Xiao *et al.* 2016). In Figure 2(b), it is found that the basic unit of flower-shaped sphere Bi_2WO_6 is a regular two-dimensional nano-sheet self-assembled in a certain order. The thickness of the film is about 50 nm, and there are large pores between the sheets. Such a flower-shaped sphere Bi_2WO_6 structure is more conducive to the adsorption of pollutants, and it can also provide more photoactive sites and optical carrier transmission routes. Therefore, flower-shaped sphere Bi_2WO_6 has higher photocatalytic activity than the one synthesized by traditional methods (Xiao *et al.* 2016). For CBW1-4, the morphology has no obvious change compared to the pure Bi_2WO_6, but the gray scale of the photos has changed, as shown in Figure 2(c) and 2(d). This is because CuS is highly dispersed on the surface of Bi_2WO_6. However, it is still difficult to observe the existence of CuS. At the surface of CBW1-4, we have carried out EDS detection, and the results are shown in Figure 2(e). By calculating the atomic percentage, we can know that CuS appears on the surface of the sample, which proves that we have successfully prepared the CBW1-4. In Figure 3, the hierarchical organization of Bi_2WO_6 nanosheets and CuS nanorods can clearly be observed. A single CuS nanorod with a length of 70–120 nm and a diameter of about 30 nm can be much visualized, as shown in Figure 3(c) and 3(d). The morphology of CuS is similar to the description in the literature (Roy *et al.* 2008). The microscopic image in Figure 3(b) shows that the CuS nanorods are in close contact with the Bi_2WO_6 nanosheets. It indicates that CuS is successfully deposited on the surface of Bi_2WO_6. The high-resolution image in Figure 3 depicts the formation of heterojunctions between the Bi_2WO_6 and CuS phases. Two different sets of lattice fringes running in different directions correspond to the (002) crystallographic plane of Bi_2WO_6 and the (103) plane of CuS.

Optical performance

The optical absorption of materials is one of the key factors for affecting the photocatalytic activity. UV–Vis absorption spectra of CuS, Bi_2WO_6 and CuS/Bi_2WO_6 are displayed in Figure 4(a). The pure Bi_2WO_6 material shows an absorption shoulder near 450 nm. The absorption shoulder for CuS commences near 650 nm. Furthermore, it can be clearly seen that, whether the absorption intensity or the location of the absorption shoulder, the pure CuS is better than the pure Bi_2WO_6 and other composite photocatalysts. Because CuS tends to be dark brown, it absorbs more light. Among the composite photocatalysts with different mass mole concentrations of CuS and Bi_2WO_6, CBW1-4 has a stronger response to visible or ultraviolet light. Moreover, the absorption edge of CBW1-4 has an obvious red shift, which indicates that it can also exhibit excellent photocatalytic activity under visible light. In the later activity testing, CBW1-4 also showed better photocatalytic activity than other composite photocatalytic cascades, and the results

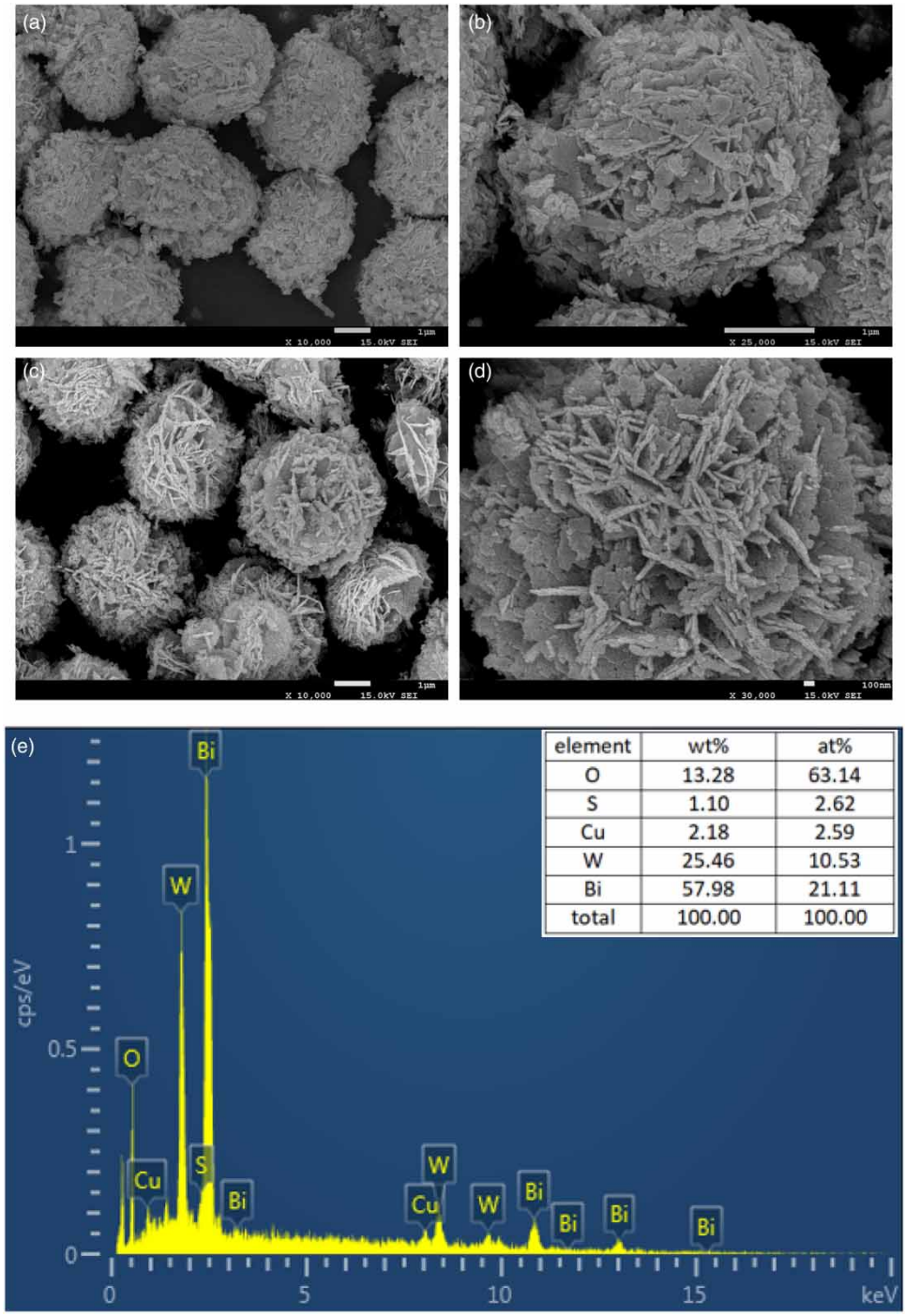

Figure 2 | SEM images of Bi_2WO_6 (a,b) and CBW1-4 (c,d). The EDS spectrum of CBW1-4 (e).

were in good agreement with UV–Vis absorption spectra. This finding indicates that the heterojunctions synthesized at the mass mole ratio of CuS to Bi_2WO_6 of 1:4 play an improved role in the catalyst.

PL spectroscopy is widely used to study carrier capture, separation and transfer efficiency. It is a simple and effective method to evaluate the recombination probability of photoelectron and hole in semiconductors. The study has shown

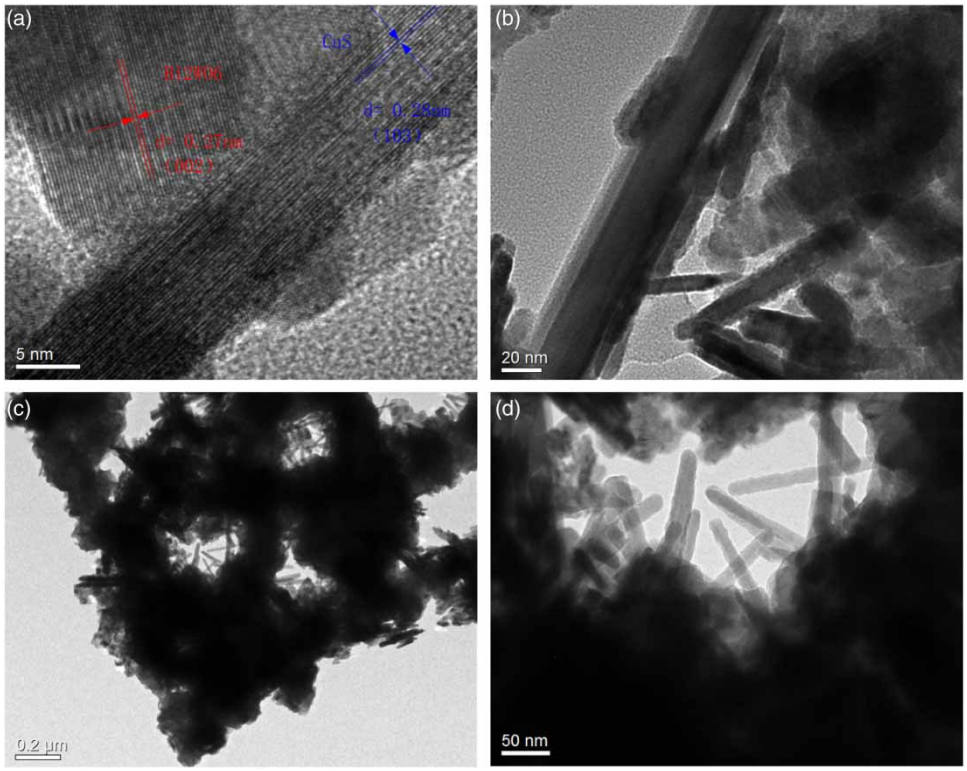

Figure 3 | HTEM image of CBW1-4.

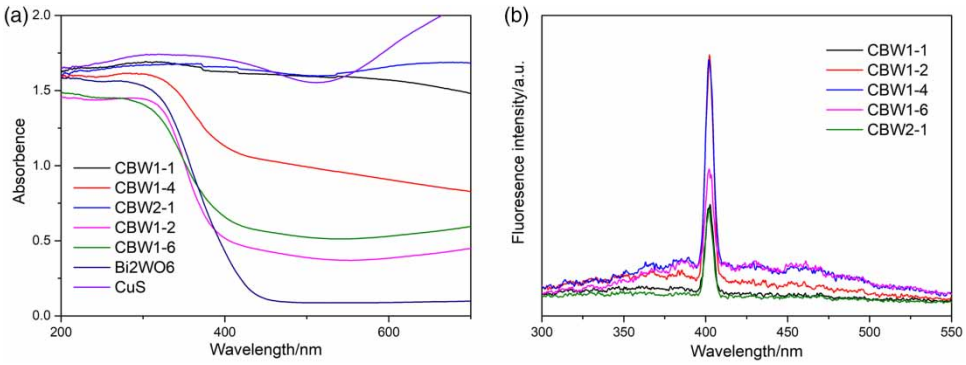

Figure 4 | UV–Vis absorption spectra (a) and PL spectra (b) of CuS, Bi_2WO_6 and CuS/Bi_2WO_6.

that when the fluorescence intensity is weaker, the recombination probability of photo-generated electrons and holes is lower (Yoshida *et al.* 2010). All CuS/Bi_2WO_6 samples are measured using an excitation wavelength of $\lambda = 200$ nm and their maximum intensity emission peaks emerge at approximately 200 nm, as illustrated in Figure 4(b). It is found that the images of CBW1-1 and CBW2-1 are lower than those of the other three catalysts, indicating that they have an obvious inhibitory effect on the combination of photo-generated electrons and photo-generated holes. In this way, they should have better photocatalytic activity. However, in the process of photocatalytic degradation of RhB, they did not perform as well as the other three photocatalysts, which indicated that the recombination rate of photo-generated carriers was only an optical property of the catalyst and would affect the photocatalytic reaction

rather than the decisive factor of the photocatalytic reaction. The success of photocatalytic reaction is the result of the synergistic action of many factors.

To identify the information on the extent of charge transfer and recombination in the samples, which influences the interfacial reactions of photoexcited electrons and the surface processes, transient photocurrent response (PC) and EIS measurement were performed under simulated solar illumination. The results are shown in Figure 5. Figure 5(a) shows the EIS spectra of CuS, Bi_2WO_6 and CBW1-4. A smaller arc size usually means a lower charge transfer resistance on the surface of materials. This arc is related to the electron transfer resistance and interfacial capacitance at the samples' electrolyte interface (Yu *et al.* 2018; Zeng *et al.* 2019). It can be seen that CBW1-4 shows the smallest impedance arc radius among all samples, implying that the combination of CuS on the surface of Bi_2WO_6 enhanced the charge transfer ability, which can be attributed to the formed heterojunction interfaces (Bajorowicz *et al.* 2015). The combination of CuS compound gives rise to a good interaction with the Bi_2WO_6, which leads to an efficient and faster charge transfer through the coupled semiconductor complex material. Figure 5(b) shows the transient PC response of Bi_2WO_6 and CBW1-4. We have tested the CuS several times, but we did not detect its PC. This result is consistent with the previous EIS profiles; the impedance of CuS is too large to produce PC under the same conditions. It can be easily seen from the figure that the PC intensity of CBW1-4 is stronger than that of Bi_2WO_6, which also shows that the addition of CuS plays an important role in increasing charge separation efficiency.

Photocatalytic studies

Photocatalytic activity

Catalytic performance is an important parameter in the evaluation of photocatalysts. After the system is stirred in the dark for 45 min to obtain adsorption equilibrium, the photocatalytic activities of Bi_2WO_6, CuS and CuS/Bi_2WO_6 with different molar mass ratios of CuS and Bi_2WO_6 under Xe lamp exposure are illustrated in Figure 6(a). It is found that both CuS and Bi_2WO_6 have lower degradation activities, respectively, corresponding to approximately 10% and 20% degradation rate of RhB after 10 min irradiation. However, the addition of CuS nanoparticles to the Bi_2WO_6 surface results in significantly improved photocatalytic effects and rates. Among all the prepared composite photocatalysts, CBW1-4 shows better photocatalytic activity than other samples and can achieve approximately 35% degradation rate of RhB within 10 min. When irradiation time increases, the RhB continues to be degraded. All the prepared photocatalysts except CBW2-1 can degrade most of the RhB in about 90 min. For CuS, only 81.3% of RhB is degraded in 90 min. Obviously, except for CBW2-1 and CBW1-1, the degradation activities of RhB over other CuS/Bi_2WO_6 samples are better than pure CuS and Bi_2WO_6, and the photocatalytic degradation efficiency of RhB increases with the increase of the Bi_2WO_6 content. When the mass mole ratio of CuS/Bi_2WO_6 is 1:4, an excellent photocatalytic activity is achieved. However, too low CuS may decrease the surface active sites of Bi_2WO_6, resulting in a decrease in the activity of CBW1-6 compared to CBW1-4 for RhB degradation.

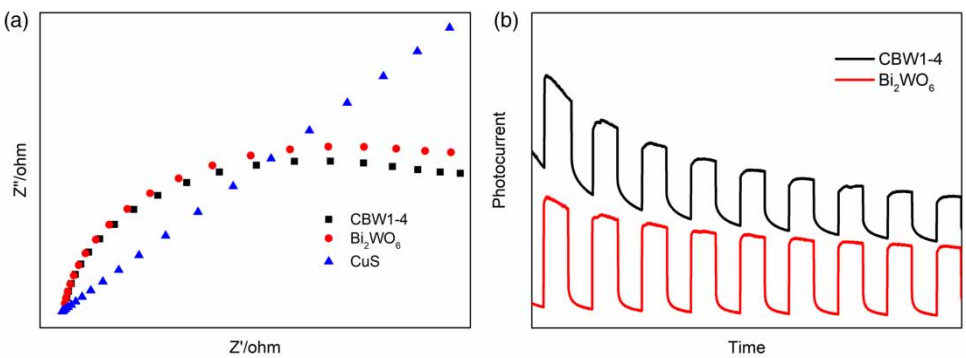

Figure 5 | Transient photocurrent response (a) and EIS profiles (b) of CuS, Bi_2WO_6 and CBW1-4.

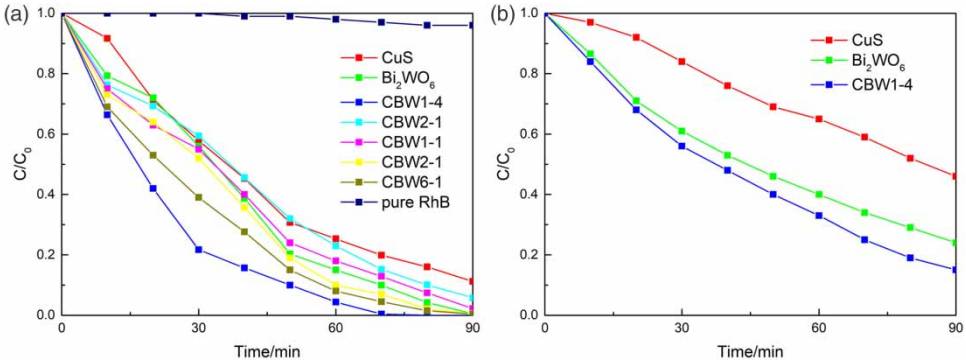

Figure 6 | Photocatalytic degradation of RhB over Bi_2WO_6, CuS, CuS/Bi_2WO_6 under Xe lamp exposure (a) and visible light (b).

Figure 6(b) shows the photocatalytic degradation of RhB over Bi_2WO_6, CuS, CuS/Bi_2WO_6 under visible light, it is obvious that the degradation ability of CBW1-4 to RhB under visible light is better than that of Bi_2WO_6 and CuS. This shows that the combination of CuS and Bi_2WO_6 can significantly improve the response of Bi_2WO_6 to visible light, resulting in enhanced degradation efficiency.

Stability and reusability

It is well known that Bi_2WO_6 is unstable in the environment of a low pH value and will be converted to tungstic acid and deactivated. Therefore, a photocatalytic reaction will not occur in a low pH environment. However, in Figure 7, the UV–Vis spectra of CBW1-4 degrading RhB in solution with pH = 3 show that CBW1-4 can still exhibit photocatalytic activity. The photocatalytic degradation of RhB over CBW1-4 under different pH conditions is illustrated in Figure 8(a). It can be seen that the photocatalytic activity of CBW1-4 for RhB increases with the decrease of pH value from 6 to 4 in the RhB solution. However, when the solution pH is equal to 3, degradation ability shows a sudden decrease. It means that CBW1-4 has lost some photocatalytic activity. This may be due to the decomposition of some Bi_2WO_6 to destroy the heterojunction formed with CuS.

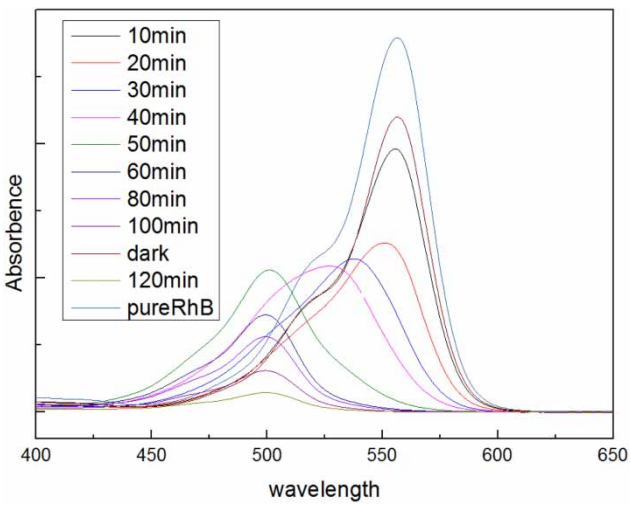

Figure 7 | The temporal evolution of UV–Vis spectra during RhB photodegradation over CBW1-4.

The quality of catalyst also depends on its stability in the process of photocatalysis. Therefore, the repeated cycle method is used to analyze the stability of the catalyst. After activity evaluation was completed, the catalysts were separated by centrifugation, washed with water and ethanol many times and dried at 80 °C. According to the photocatalytic activity described in the experimental part, the photodegradation of RhB in solution without adjusting the pH is tested over the used catalysts for multiple recycling and the results are shown in Figure 8(b). It is found that the changing trend of RhB degradation with time compared to CBW1-4 is similar. In addition, after four cycles, the degradation efficiency of the photocatalyst decreased slightly. These findings indicate that the CBW1-4 photocatalysts can remain stable. Therefore, the prepared CBW1-4 photocatalysts are reusable and cost-effective.

Kinetics

The photodegradation rates of CuS, Bi_2WO_6 and CBW1-4 could be calculated via a pseudo-first-order kinetics model

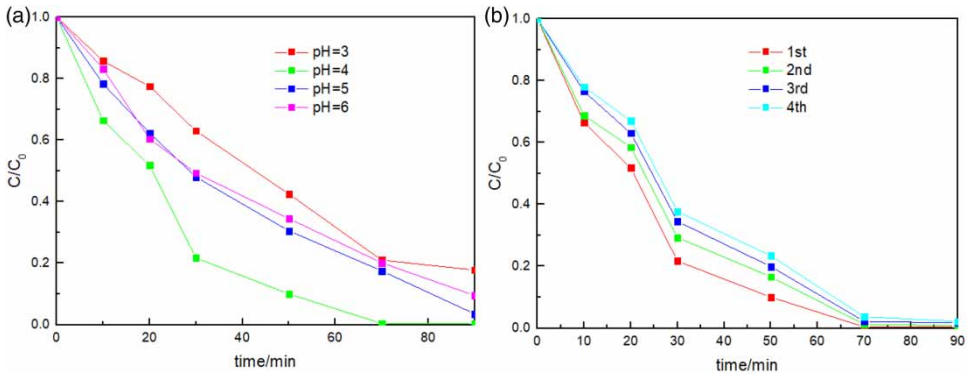

Figure 8 | RhB photocatalytic degradation over CBW1-4 under different pH conditions (a) and cycling runs (b).

as follows:

$$\ln(C_0/C_t) = kt$$

where C_0 (mg/L) and C_t (mg/L) are the concentrations of RhB at the reaction time (t; min). The plots of RhB concentration versus irradiation time and the rate constant are shown in Figure 9. It is found that the CBW1-4 sample reveals a higher degradation rate than pure CuS and Bi_2WO_6 under Xe lamp irradiation. The rate constant k of CBW1-4 is 0.0595 min^{-1}, which is 3.3 times and 1.5 times as high as that of the pure CuS and CuS/Bi_2WO_6. This finding indicates that the combination of CuS and Bi_2WO_6 and the formation of heterojunction structures between CuS and Bi_2WO_6 enhance the photocatalytic activity.

Mechanism study

In the photocatalytic degradation process of RhB dyes, photoexcited semiconductors produce electrons and holes and then generate various active substances to participate in the degradation process of RhB. The photocatalytic degradation process usually includes the following reaction steps:

$$\text{Catalyst} \rightarrow e^- + h^+ \quad (1)$$

$$e^- + O_2 \rightarrow \bullet O_2^- \quad (2)$$

$$h^+ + H_2O \rightarrow \bullet OH + H^+ \quad (3)$$

$$h^+ + OH^- \rightarrow \bullet OH \quad (4)$$

$$RhB + \bullet O_2^- \rightarrow \text{Products} \quad (5)$$

$$RhB + \bullet OH \rightarrow \text{Products} \quad (6)$$

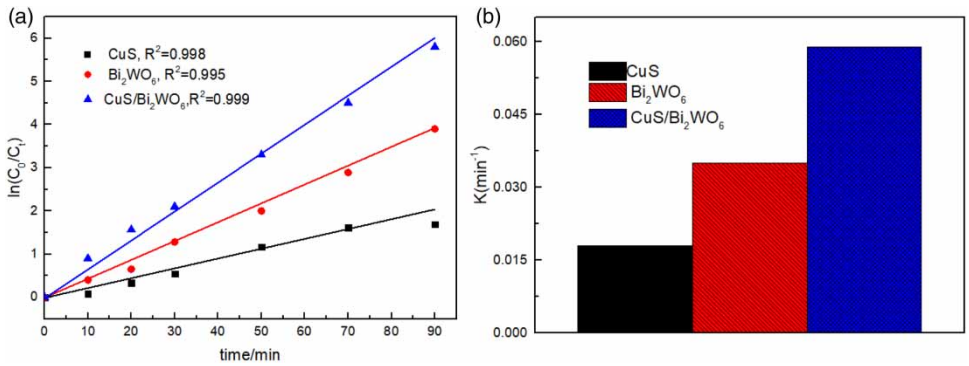

Figure 9 | Kinetics (a) and rate constant chart (b) of RhB degradation over CuS, Bi_2WO_6 and CBW1-4.

The semiconductor photocatalyst generates photogenerated electrons and holes after being exposed to light. The electrons excited to the bottom of the conduction band (CB) can form superoxide radical ($\cdot O_2^-$) with O_2 on the surface of the catalyst. This $\cdot O_2^-$ is very active. It can oxidize the adsorbed RhB to mineralize it into CO_2 and H_2O. At the same time, the holes left at the top of the valence band (VB) can react directly with RhB or with H_2O or OH^- to produce hydroxyl radicals (•OH) (Czapski 1984). This •OH can indirectly mineralize RhB. In order to understand the role of various active species in the photocatalytic reaction of RhB in this system, free radical and hole scavenging experiments were carried out during the process of degradation with CBW1-4. In this study, isopropanol (IPA), methanol (MeOH) and *p*-benzoquinone (BQ) are used as •OH radical scavenger, hole (h^+) scavenger and $\cdot O_2^-$ radical scavenger (Viggiano *et al.* 1988), respectively. The concentration of these scavengers is 1 mmol/L.

The effects of various scavengers on the photocatalytic activity of CBW1-4 in the same reaction system under Xe lamp irradiation are shown in Figure 10(a). Compared with the scavenger-free CBW1-4 photocatalytic system, the degradation rate of RhB is obviously inhibited after the addition of IPA during the entire test period. For the BQ-CBW1-4 photocatalytic system, there is little effect on the photocatalytic degradation rate of RhB before 10 min, but as time increases, the degradation of RhB is inhibited greatly. As for the MeOH-CBW1-4 photocatalytic system, the degradation rate of RhB obviously increases before 30 min; the degradation of RhB is inhibited greatly in the range of 30–60 min; and after 60 min, the degradation of RhB is the same as that of the scavenger-free system. The above results indicate that the •OH radical is hardly generated, while the $\cdot O_2^-$ radical is the significant active species generated in the CBW1-4–photocatalytic system. As for h^+, it can be scavenged in the presence of MeOH, so more e− can react with O_2 to form $\cdot O_2^-$ instead of

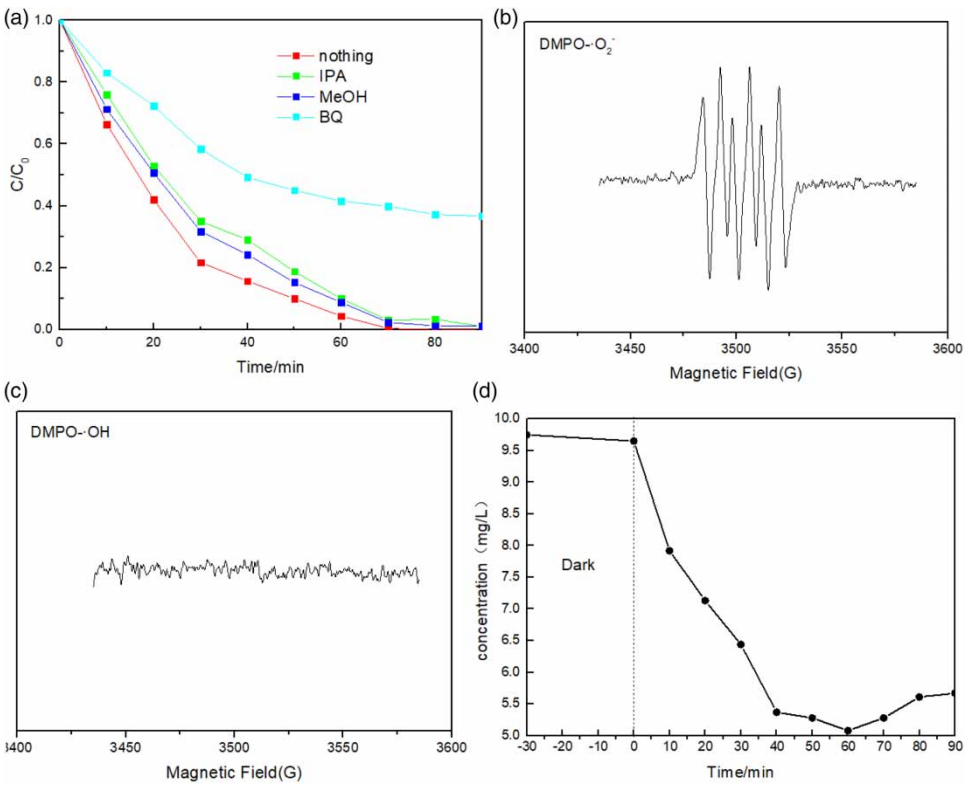

Figure 10 | Influence of various scavengers on the photocatalytic activity during degradation of RhB over CBW1-4 (a); ESR spectra of CBW1-4 after Xe lamp light irradiation: DMPO-•O_2^- in methanol dispersion (b) and DMPO-•OH in aqueous dispersion (c); and changes of the dissolved oxygen in solution during degradation of RhB over CBW1-4 (d).

the rapid recombination with h^+ [Equation (2)], which further improves the photocatalytic activity. It also suggests that h^+ and •OH are not the main active substances in the photocatalytic reaction process, whereas $\cdot O_2^-$ plays a decisive role in the photocatalytic degradation of RhB in this reaction system. In order to verify the above results, the ESR spin-trap with the DMPO technique was carried out. As shown in Figure 10(b) and 10(c), when the samples are exposed to the Xe lamp irradiation, the typical signals of $\cdot O_2^-$ and •OH are detected in water and in methanol solution, respectively. Furthermore, the ERS signal of $\cdot O_2^-$ is much stronger than that of •OH under the Xe lamp irradiation. Therefore, it can be explained that the ESR results are in good agreement with the above experimental results.

In order to study the consumption of oxygen in the photocatalytic system, the dissolved oxygen in the RhB solution during the reaction process was also detected. As shown in Figure 10(d), the decrease of the dissolved oxygen content in the solution during the dark reaction is not obvious, which indicates that the photocatalyst mainly adsorbs RhB while the oxygen adsorbed can be neglected in this process. When the solution is irradiated by a Xe lamp, the dissolved oxygen content in the solution decreases obviously, suggesting that the photocatalytic reaction is taking place. At this time, the dissolved oxygen participates in the photocatalytic reaction. It can combine with transitional electrons on the surface of the catalyst to form $\cdot O_2^-$. This $\cdot O_2^-$ participates in the degradation of RhB. However, when RhB is completely degraded, the dissolved oxygen

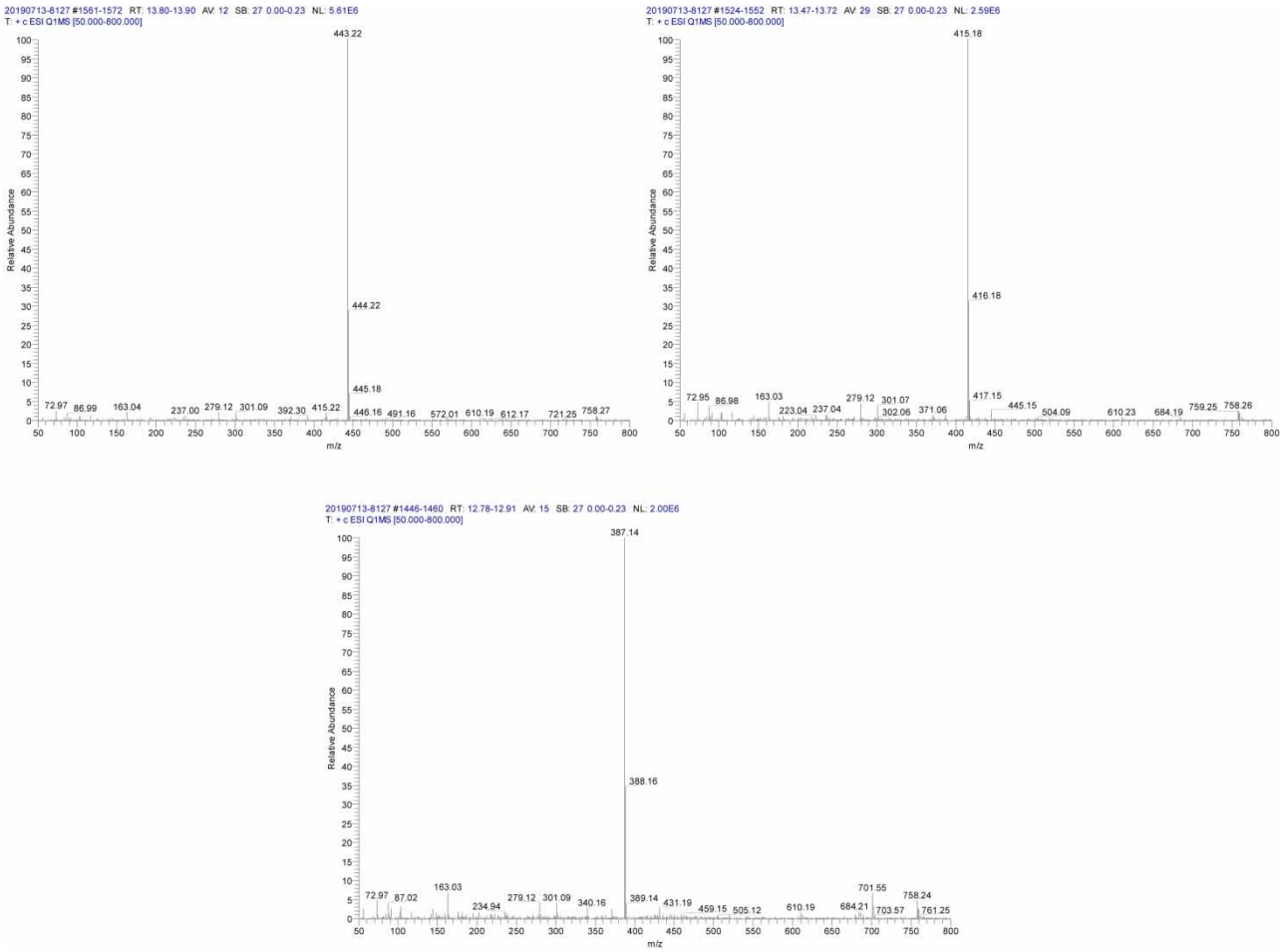

Figure 11 | LC–MS analysis of intermediate products during degradation of RhB.

content in the solution does not decrease but rises slowly. This is because the oxygen in the air can be dissolved into the solution when the solution is constantly stirred. Stirring accelerates the mass transfer between the liquid and the gas. This work can also show the validity of the above experimental mechanism inference.

The degradation pathway of RhB is also studied in this paper. Generally, in the photocatalytic degradation of RhB, the N-de-ethyl reaction and the ring-opening reaction of the benzene ring are carried out simultaneously. On the surface of the photocatalyst, the N-de-ethyl reaction is dominant, while in solution, the ring-opening reaction of the benzene ring is dominant (Dong *et al.* 2016). In the suspension system formed by the CuS/Bi_2WO_6 photocatalyst and RhB solution, the N-de-ethyl reaction and the ring-opening reaction are carried out simultaneously. It can be seen from Figure 7 that the maximum absorption peak shifted to blue at the beginning of the reaction, and then the maximum absorption peak remained unchanged. As the light progressed, the height continued to decline until the degradation was completed. In order to study the intermediate products in the degradation of RhB, the solution in the reaction was characterized by LC–MS. The results are shown in Figure 11. We found in the ionic spectra the ion peaks are mainly the products of RhB (443) and N-de-ethylated products, 415 for the *N*,*N*-diethyl-*N*'-ethyl rhodamine (DER) and 387 for the *N*-ethyl-*N*'-ethyl rhodamine (EER). The ion peaks of the products further degraded are very few and the intensity of the ion peaks is very weak. This is because the small molecules formed by the opening of the benzene ring are easily oxidized by the active species O_2^- in this system; the life of those molecules is very short. Therefore, these small molecules cannot exist in the solution or the concentration is very low. They are obviously detected by LC–MS. The probable reaction pathway of the RhB solution in photocatalytic degradation by CuS/Bi_2WO_6 can be proposed. As shown in Figure 12, RhB firstly takes off one ethyl from -N linked to the benzene ring to form DER, and then DER takes off another ethyl to form EER. Finally, the DER and EER can further carry out ring-opening reactions. In addition, the de-ethylation and ring-opening reactions simultaneously produce other small organic molecules. Those small organic molecules generated are oxidized rapidly to H_2O or CO_2 in the presence of O_2^- in the solution.

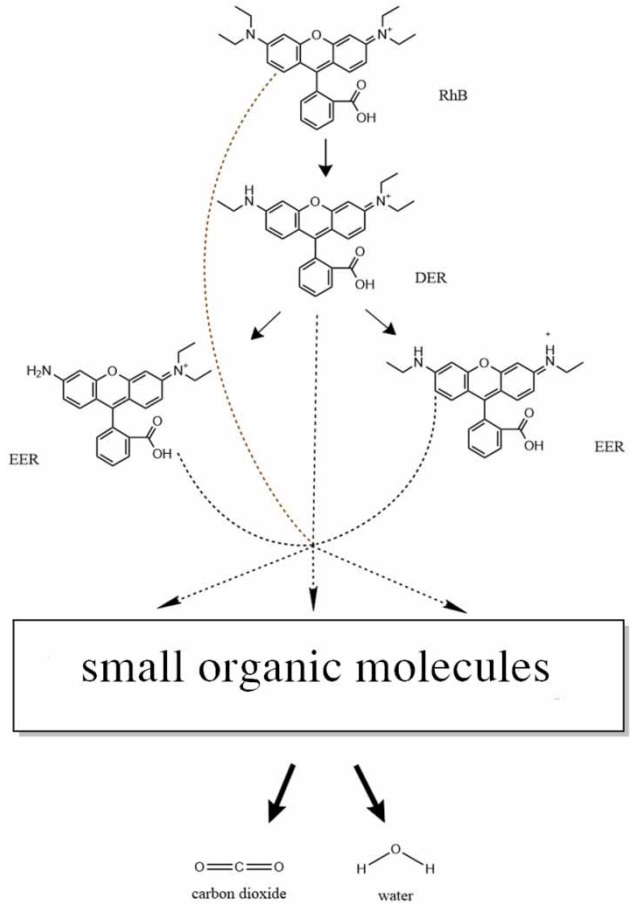

Figure 12 | Photocatalytic degradation pathway of RhB.

DISCUSSION

Based on the above experimental results, the enhanced photocatalytic activity of CuS/Bi_2WO_6 and the possible mechanism of RhB degradation are proposed, as shown in Figure 13. Before illumination, electrons and holes combine to form electron–hole pairs in the VB. Under light irradiation, electrons are excited to the CB due to the absorption of light energy, and the holes are left in the VB band (Min *et al.* 2012; Dong *et al.* 2019c). Both CuS and Bi_2WO_6 can be excited by light at the same time to produce electrons and holes under light irradiation. However, the positively charged holes and the negatively charged electrons attract each other, resulting in rapid recombination. This causes low RhB degradation efficiency of single CuS and Bi_2WO_6. When

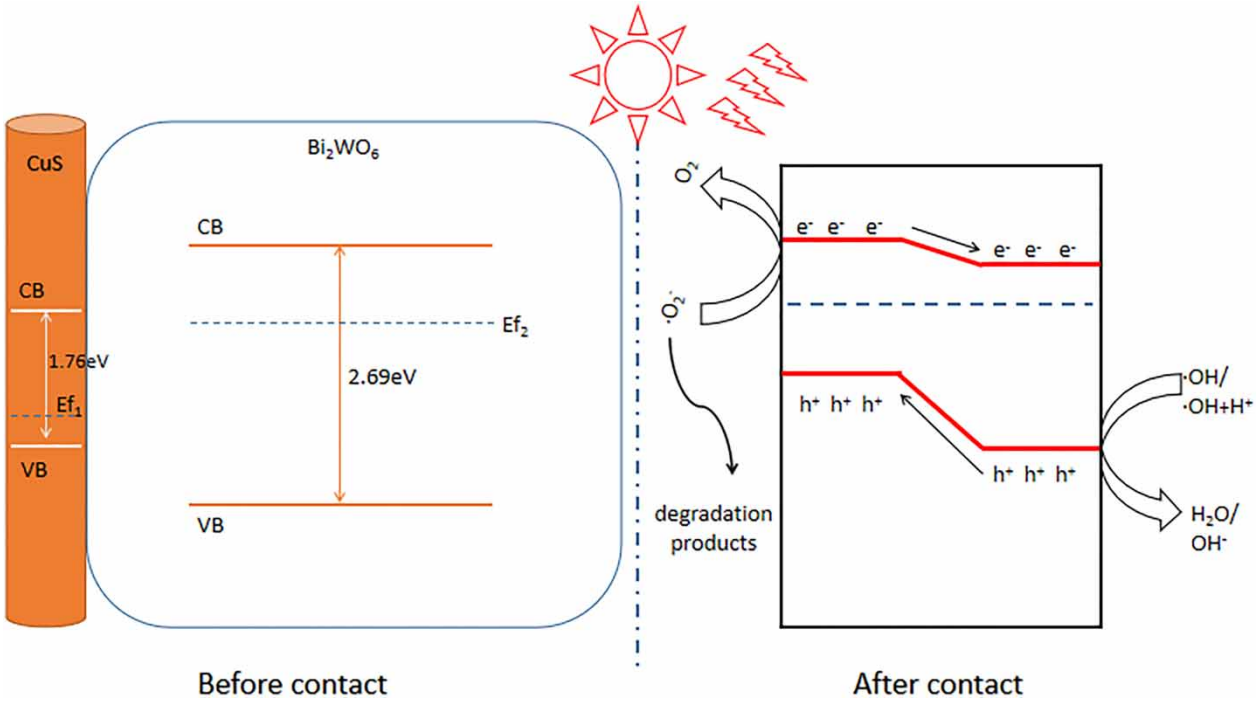

Figure 13 | Schematic diagram showing the separation of photo-generated charge carriers over the CuS/Bi_2WO_6 heterojunction.

N-type semiconductor Bi_2WO_6 and P-type semiconductor CuS are combined to form a new heterogeneous junction, the valence and conduction bands of these two semiconductors migrate until their Fermi levels are consistent (Mao *et al.* 2011), which would lead to the improved catalytic activity observed by increasing the separation efficiency of holes and electrons. According to the energy band relationship after recombination, the photo-generated holes migrate from the VB of Bi_2WO_6 to the VB of CuS, while the photo-generated electrons migrate from the CB of CuS to the CB of Bi_2WO_6. Since negatively charged electrons accumulate on the CB of Bi_2WO_6 with potential correction, compared to the holes accumulated on the VB of CuS, they are more active and easily generate $\cdot O_2^-$ with the absorbed oxygen. Therefore, $\cdot O_2^-$ becomes the main active species in the photocatalytic process of this system. Because of the presence of O_2^-, small organic molecules produced in the RhB degradation process are rapidly degraded to CO_2 and H_2O, which significantly enhances the photocatalytic efficiency.

CONCLUSION

In this work, a novel CuS/Bi_2WO_6 with flower-shaped nanosphere and a heterojunction structure is successfully synthesized by a solvent synthesis method. The heterojunction catalysts CuS/Bi_2WO_6 exhibit higher photocatalytic activity than pure Bi_2WO_6 and CuS for the degradation of RhB under Xe lamp irradiation, and it shows optimal activity when the mass mole ratio of CuS and Bi_2WO_6 is 1–4. Compared with pure Bi_2WO_6, the CBW1-4 photocatalyst can stably participate in the photocatalytic reaction under acidic conditions and demonstrate better photocatalytic performance in the degradation of RhB. The existence of CuS improves the migration efficiency of electrons and holes in CBW1-4 and reduces the possibility of electrons and holes recombination. The major active species of CBW1-4 in photocatalytic degradation of the RhB process is $\cdot O_2^-$ species, and oxygen can be adsorbed on the surface of CBW1-4 and get two e^- to become $\cdot O_2^-$ in this reaction system under illumination, thus rapidly degrading RhB directly.

ACKNOWLEDGEMENTS

This work is financially supported by the Sichuan Provincial Science and Technology Agency Support Projects (No. 2017GZ0379).

REFERENCES

Bajorowicz, B., Reszczyńska, J., Lisowski, W., Klimczuk, T., Winiarski, M., Słoma, M. & Zaleska-Medynska, A. 2015 Perovskite-type $KTaO_3$–reduced graphene oxide hybrid with improved visible light photocatalytic activity. *RSC Advances* **5** (111), 91315–91325.

Chen, Q., Wu, S. & Xin, Y. 2016 Synthesis of Au–CuS–TiO_2 nanobelts photocatalyst for efficient photocatalytic degradation of antibiotic oxytetracycline. *Chemical Engineering Journal* **302**, 377–387.

Chen, P., Xing, P., Chen, Z., Hu, X., Lin, H., Zhao, L. & He, Y. 2019a In-situ synthesis of $AgNbO_3$/g-C_3N_4 photocatalyst via microwave heating method for efficiently photocatalytic H2 generation. *Journal of Colloid and Interface Science* **534**, 163–171.

Chen, P., Dai, X., Xing, P., Zhao, X., Zhang, Q., Ge, S. & He, Y. 2019b Microwave heating assisted synthesis of novel SnSe/g-C_3N_4 composites for effective photocatalytic H_2 production. *Journal of Industrial and Engineering Chemistry* **80**, 74–82.

Chong, M. N., Jin, B., Chow, C. W. & Saint, C. 2010 Recent developments in photocatalytic water treatment technology: a review. *Water Research* **44**, 2997–3027.

Czapski, G. 1984 Reaction of •OH. *Methods in Enzymology* **105**, 209–215.

Ding, T. Y., Wang, M. S., Guo, S. P., Guo, G. C. & Huang, J. S. 2008 Cus nanoflowers prepared by a polyol route and their photocatalytic property. *Materials Letters* **62**, 4529–4531.

Dong, S., Pi, Y., Li, Q., Hu, L., Li, Y., Han, X. & Sun, J. 2016 Solar photocatalytic degradation of sulfanilamide by BiOCl/reduced graphene oxide nanocomposites: mechanism and degradation pathways. *Journal of Alloys and Compounds* **663**, 1–9.

Dong, S., Ding, X., Guo, T., Yue, X., Han, X. & Sun, J. 2017 Self-assembled hollow sphere shaped Bi_2WO_6/RGO composites for efficient sunlight-driven photocatalytic degradation of organic pollutants. *Chemical Engineering Journal* **316**, 778–789.

Dong, S., Xia, L., Zhang, F., Li, F., Wang, Y., Cui, L. & Sun, J. 2019a Effects of pH value and hydrothermal treatment on the microstructure and natural-sunlight photocatalytic performance of $ZnSn(OH)_6$ photocatalyst. *Journal of Alloys and Compounds* **810**, 151955.

Dong, S., Cui, L., Liu, C., Zhang, F., Li, K., Xia, L. & Sun, J. 2019b Fabrication of 3D ultra-light graphene aerogel/Bi_2WO_6 composite with excellent photocatalytic performance: a promising photocatalysts for water purification. *Journal of the Taiwan Institute of Chemical Engineers* **97**, 288–296.

Dong, S., Cui, L., Zhao, Y., Wu, Y., Xia, L., Su, X. & Sun, J. 2019c Crystal structure and photocatalytic properties of perovskite $MSn(OH)_6$ (M = Cu and Zn) composites with d10-d10 configuration. *Applied Surface Science* **463**, 659–667.

Feng, Z., Zeng, L., Zhang, Q., Ge, S., Zhao, X., Lin, H. & He, Y. 2020 In situ preparation of g-C3N4/$Bi_4O_5I_2$ complex and its elevated photoactivity in Methyl Orange degradation under visible light. *Journal of Environmental Sciences* **87**, 149–162.

Herrmann, J. M., Guillard, C. & Pichat, P. 1993 Heterogeneous photocatalysis: an emerging technology for water treatment. *Catalysis Today* **17**, 7–20.

Inoue, S., Ueda, K., Hosono, H. & Hamada, N. 2001 Electronic structure of the transparent p-type semiconductor (LaO)CuS. *Physical Review B* **64**, 245211.

Ismail, A. A., Al-Sayari, S. A. & Bahnemann, D. W. 2013 Photodeposition of precious metals onto mesoporous TiO_2 nanocrystals with enhanced their photocatalytic activity for methanol oxidation. *Catalysis Today* **209**, 2–7.

Kuchment, P. & Kunyansky, L. 1999 Spectral properties of high contrast band–gap materials and operators on graphs. *Experimental Mathematics* **8** (1), 1–28.

Lefebvre, O. & Moletta, R. 2006 Treatment of organic pollution in industrial saline wastewater: a literature review. *Water Research* **40**, 3671–3682.

Li, L., Chu, Y., Liu, Y. & Dong, L. 2007 Template–free synthesis and photocatalytic properties of novel Fe_2O_3 hollow spheres. *Journal of Physical Chemistry C* **111**, 2123–2127.

Li, G. S., Zhang, D. Q. & Yu, J. C. 2009 A new visible–light photocatalyst: CdS quantum dots embedded mesoporous TiO_2. *Environmental Science & Technology* **43**, 7079–7085.

Mao, H. Y., Bussolotti, F., Qi, D. C., Wang, R., Kera, S. & Ueno, N. 2011 Mechanism of the Fermi level pinning at organic donor–acceptor heterojunction interfaces. *Organic Electronics* **2**, 534–540.

Min, Y., Zhang, K., Chen, Y., Zhang, Y. & Zhao, W. 2012 Synthesis of nanostructured ZnO/Bi_2WO_6 heterojunction for photocatalysis application. *Separation and Purification Technology* **92**, 115–120.

Musikavong, C., Wattanachira, S., Marhaba, T. F. & Pavasant, P. 2005 Reduction of organic matter and trihalomethane formation potential in reclaimed water from treated industrial estate wastewater by coagulation. *Journal of Hazardous materials* **127**, 58–67.

Oregan, B. & Schwartz, D. T. 1996 Efficient dye-sensitized charge separation in a wide-band-gap p-n heterojunction. *Journal of Applied Physics* **80**, 4749–4754.

Roy, P., Mondal, K. & Srivastava, S. K. 2008 Synthesis of twinned CuS nanorods by a simple wet chemical method. *Crystal Growth and Design* **8**, 1530–1534.

Saranya, M., Ramachandran, R., Samuel, E. J. J., Jeong, S. K. & Grace, A. N. 2015 Enhanced visible light photocatalytic

reduction of organic pollutant and electrochemical properties of CuS catalyst. *Powder Technology*. **279**, 209–220.

Shi, Y., Hua, C., Li, B., Fang, X., Yao, C. & Zhang, Y. 2013 Highly ordered mesoporous crystalline MoSe material with efficient visible–light–driven photocatalytic activity and enhanced lithium storage performance. *Advanced Functional Materials* **23**, 1832–1838.

Tang, L., Wang, J., Zeng, G., Liu, Y., Deng, Y., Zhou, Y., Tang, J., Wang, J. & Guo, Z. 2016 Enhanced photocatalytic degradation of norfloxacin in aqueous Bi_2WO_6 dispersions containing nonionic surfactant under visible light irradiation. *Journal of Hazardous materials* **306**, 295–304.

Tristão, J. C., Magalhães, F., Corio, P. & Sansiviero, M. T. C. 2006 Electronic characterization and photocatalytic properties of CdS/TiO_2 semiconductor composite. *Journal of Photochemistry and Photobiology A: Chemistry* **181**, 152–157.

Viggiano, A. A., Dale, F. & Paulson, J. F. 1988 Proton transfer reactions of $H(+)(H_2O)n = 2$-11 with methanol, ammonia, pyridine, acetonitrile, and acetone. *Journal of Chemical Physics* **88**, 2469–2477.

Wan, J., Du, X., Wang, R., Liu, E., Jia, J., Bai, X., Hu, X. & Fan, J. 2018 Mesoporous nanoplate multi-directional assembled Bi_2WO_6 for high efficient photocatalytic oxidation of NO. *Chemosphere* **193**, 737–744.

Würthner, F., Chen, Z., Hoeben, F. J. M., Osswald, P., You, C. C. & Jonkheijm, P. 2004 Supramolecular p-n-heterojunctions by co-self-organization of oligo (p-phenylene vinylene) and perylene bisimide dyes. *Journal of the American Chemical Society* **126**, 10611–10618.

Xiao, J., Song, C., Dong, W., Yin, Y. & Li, C. 2016 Preparation and gas sensing properties of hierarchical flower-shaped Bi_2WO_6. *Australian Journal of Chemistry* **69**, 107.

Yoshida, M., Hirai, T. & Maeda, K. 2010 Photoluminescence spectroscopic and computational investigation of the origin of the visible light response of $(Ga_{1-x}Zn_x)(N_{1-x}O_x)$ photocatalyst for overall water splitting. *Journal of Physical Chemistry C* **114**, 15510–15515.

Yu, J., Chen, Z., Zeng, L., Ma, Y., Feng, Z., Wu, Y. & He, Y. 2018 Synthesis of carbon-doped $KNbO_3$ photocatalyst with excellent performance for photocatalytic hydrogen production. *Solar Energy Materials and Solar Cells* **179**, 45–56.

Zeng, L., Zhe, F., Wang, Y., Zhang, Q., Zhao, X., Hu, X. & He, Y. 2019 Preparation of interstitial carbon doped BiOI for enhanced performance in photocatalytic nitrogen fixation and methyl orange degradation. *Journal of Colloid and Interface Science* **539**, 563–574.

Zhang, L., Wang, W., Zhou, L. & Xu, H. 2010 Bi_2WO_6 nano-microstructures: shape control and associated visible–light–driven photocatalytic activities. *Small* **3**, 1618–1625.

Zheng, H., Guo, W., Li, S., Yin, R., Wu, Q., Feng, X., Ren, N. & Chang, J. S. 2017 Surfactant (CTAB) assisted flower-like Bi_2WO_6 through hydrothermal method: unintentional bromide ion doping and photocatalytic activity. *Catalysis Communications* **88**, 68–72.

Zheng, Y., Tan, G., Bo, H., Xia, A. & Ren, H. 2011 Effect of pH value on synthesis of Bi_2WO_6 powders by microwave hydrothermal method and photocatalytic properties. *Journal of the Chinese Ceramic Society* **39**, 481–485.

First received 22 August 2019; accepted in revised form 2 December 2019. Available online 3 February 2020